Dynamic behavior modelling of a hybrid magnetorheological elastomer with encapsulated fluid for base vibration isolation

Abdelrahman Ali, Asan G.A. Muthalif [*]

Department of Mechanical and Industrial Engineering, College of Engineering, Qatar University, Doha, P.O. Box 2713, Qatar

ARTICLE INFO

ABSTRACT

Magnetorheological elastomers (MRE) based semi-active isolators utilize MREs whose mechanical properties, such as stiffness and damping, change in response to an external magnetic field. MREs implementation in semi-active isolation remains challenging due to their slow response time caused by the suspension of the magnetic particles inside the elastomeric matrix and limited damping capabilities. Hybrid MREs, a combination of MREs and MRFs, have been developed to improve semi-active isolation's material properties and performance. However, modelling the nonlinear and hysteretic behavior of hybrid MRE-based isolators remains a challenge and needs to be adequately addressed. To bridge the gap, this study presents a parametric model for a hybrid semi-active isolator's nonlinear and hysteretic behavior that utilizes a hybrid MRE (H-MRE). The behavior of conventional and hybrid MRE-based isolators are experimentally tested under varying loading conditions of excitation frequency and input current. Simulation models are created using combinations of three different phenomenological models, Bouc-Wen, Modified-Dahl and LuGre friction. The experimental data are used to optimize and fit the simulated response of each model, and hence optimal values of the MRE and MRF hysteresis parameters are determined. The parameter estimation results indicate that a combination of LuGre friction for the MRE and Bouc-Wen for the MRF improves the accuracy of predicting the dynamic behaviour of the hybrid isolator. The relationship between the model parameters and loading conditions is also investigated and described through polynomial equations of the third order. These findings could provide valuable insights for the system identification and control of hybrid semi-active isolators and pave the way for developing smart base isolation systems utilizing hybrid MREs in future research.

1. Introduction

Magnetorheological elastomers (MREs) are a type of smart material made of magnetizable particles suspended in elastomeric matrix. MREs exhibit a change in their mechanical properties, such as stiffness and damping, in response to an applied magnetic field (Carlson and Jolly, 2000), (Choi et al., 2014). When an external magnetic field is applied to the material, the magnetic particles within the MRE align along the field lines. Upon removal of the magnetic field, the MRE quickly returns to its original microstructure. This property, known as the magnetorheological (MR) effect, is a result of the alignment of the magnetic particles in response to the field (Hafeez et al., 2020); (Díez et al., 2021)–(Ubaidillah et al., 2015). The alignment of these particles can be used to control the material's mechanical properties, making it a highly versatile material with a wide range of potential applications, including damping, actuation (Khurana et al., 2022a), (Khurana et al., 2021), and

sensing (Jang et al., 2018), (Koo et al., 2012). Many studies have focused on the testing and potential applications of MREs. Particularly, the semi-active isolation devices using MREs received much attention in recent decades. This is because semi-active isolation devices are a hybrid of passive and active devices. While active isolation devices are effective at achieving high isolation levels, they can be expensive, require a lot of power, and be complex to implement. Passive isolation devices are simple and easy to implement but lack adaptability. Semi-active isolation bridges the gap between both devices by being able to adjust in real-time without needing a lot of power. Such devices rely on the system's inherent properties and can be implemented using smart materials such as MREs (Gao et al., 2019)– (Sun et al., 2014); (Salem et al., 2021).

Despite the inherent property-change characteristics of MREs, their implementation in semi-active isolation remains challenging due to their slow response time and suspension of the magnetic particles inside the elastomeric matrix, which limit the range of their stiffness change
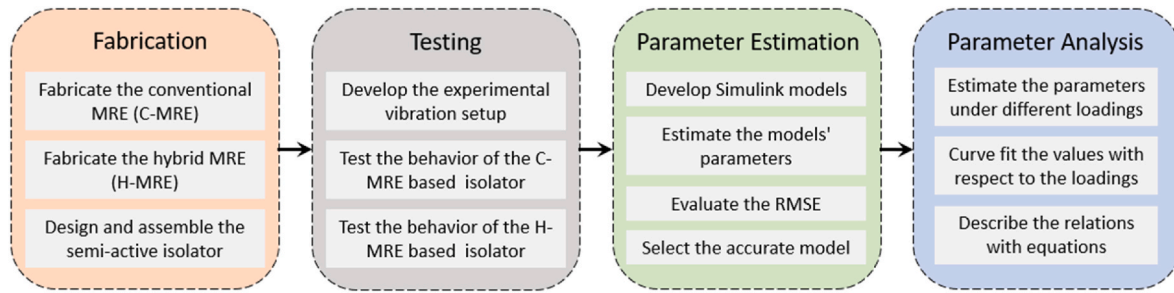

Fig. 1. Overview of the methodology.

([Bastola and Hossain, 2020](#)), ([Kang et al., 2020](#)). For this reason, hybrid MREs have been developed by integrating MREs with their fluid counterparts, MRFs. The hybrid materials have been fabricated by encapsulating the viscus MR fluid inside the elastomer matrix by direct molding or 3D printing ([Bastola et al., 2018](#))– ([Ali et al., 2022](#)); ([Qi et al., 2020](#)). By combining the properties of both materials, the hybrid MREs can exhibit a wider range of mechanical properties and respond faster to the magnetic field. Thus, hybrid MREs potentially have improved the performance in semi-active vibration isolation.

Although the hybrid MRE-based semi-active isolators have a high potential in vibration control, the main challenge remains in modelling the nonlinear and hysteretic behavior of these semi-active devices. It is important to develop a reliable model of their behavior to design effective control methods for hybrid MRE-based isolators. However, relatively few models have been proposed for the hybrid MRE-based isolators working with both elastomer and fluid, and more research is particularly needed in this area. Dynamic studies and modeling are essential for understanding the behavior of MREs that can change their stiffness and damping properties in response to an applied magnetic field. Through dynamic studies, researchers can investigate the time-dependent mechanical response of MREs under various loading conditions and magnetic fields. Modeling, on the other hand, allows the prediction of the behavior of MREs before conducting physical experiments. By combining both approaches, researchers can gain a deeper understanding of MREs' properties, enabling them to optimize the material's design and performance for various applications. Dynamic studies and modeling can help improve the development of MRE-based vibration dampers and seismic isolation systems ([Khurana et al., 2022b](#)).

Two main classes of models have been proposed for the conventional MRE-based isolators: nonparametric and parametric models. Nonparametric modeling, which uses artificial intelligence methods and can provide accurate and adaptable predictions of device responses, has been developed using neural networks and support vector regression. Such an approach does not rely on predetermined functions or equations. Instead, nonparametric models learn the underlying relationships between the input variables (e.g., the applied magnetic field) and the output variables (e.g., the stiffness of the MRE) directly from the training data, which necessary to use training data to adjust the parameters of the model and accurately predict the behavior. Nonparametric models can be more flexible and able to capture complex relationships; nevertheless, they may require more tuning data to achieve good predictions.

Additionally, these models lack physical meaning in their model parameters. It is desirable to have a model that can clearly link its parameters' physical explanation to the material's hysteretic responses. On the other hand, parametric modelling involves using a set of predetermined functions or equations to describe the behavior of the MREs. These functions are typically chosen based on physical principles or empirical observations, and the parameters of the functions are estimated from experimental data. Hence, parametric models can address the issue of having physically interpretable parameters for modeling MRE-based isolators.

Among the parametric models, the Bouc-Wen model is widely used

and well-known for describing the behavior of systems with hysteresis, such as MREs ([Li and Li, 2019](#)). The Bouc-Wen model is typically expressed as a set of differential equations describing the relationship between the input (e.g., the applied force) and the system's output (e.g., the displacement). One of its key advantages is that it can capture both the nonlinear stiffness and hysteretic behavior of MREs. It is based on the concept of an equivalent linear spring-dashpot system, with the spring representing the stiffness of the material and the dashpot representing the energy dissipation due to hysteresis. In addition to the Bouc-Wen model, two other parametric models have been proposed for modelling MRE behavior. One of these is the Dahl model, developed to describe MRE behaviour. It uses the Dahl hysteretic component instead of the Bouc-Wen component to simulate the shear force, which helps to reduce the number of parameters that need to be identified ([Zhou et al., 2006](#)), ([Li et al., 2014](#)). The Dahl model has been shown to accurately reproduce the force-displacement responses of MREs in the peak displacement regions. Another parametric model has been proposed for modeling the behavior of MREs, known as the LuGre hysteretic model. This model uses the LuGre component to capture the shear dynamics of MREs and has a relatively simple configuration compared to the Bouc-Wen model ([Jiménez and Álvarez-Icaza, 2005](#)), ([Yu et al., 2015](#)). Despite its simplicity, the LuGre model can be linearized through appropriate operation, making it suitable for real-time parameter identification.

The above models can accurately simulate semi-active isolators' dynamic and hysteretic behaviors. However, as mentioned earlier, there are currently limited models for hybrid MRE-based isolators that incorporate elastomer and fluid with hysteretic behavior. Additionally, the current models that works solely for MRE or MRFs can have large errors and be computationally expensive when trying to optimize model parameters using methods such as genetic algorithms, particle swarm optimization, and fruit fly optimization during parameter identification phase ([Muthalif et al., 2021](#)). Moreover, these models are also specific to certain types of loading excitation and need to be recalculated if the excitation is changed. Therefore, a generalized model is needed to address these issues that can accommodate various excitation conditions, such as a sinusoidal excitation with a fixed frequency, amplitude, and current level.

In this study, a parametric model is developed to effectively predict the dynamic and hysteretic behavior of a semi-active isolator working with MRE and MRF components. To achieve this model, a hybrid MRE is first fabricated by encapsulating MR fluid inside the elastomeric matrix through direct molding. Then, experiments are conducted to evaluate the performance of the hybrid MRE-based semi-active isolator under different excitation conditions, including varying frequencies, amplitudes, and currents. Secondly, generalized models are constructed, incorporating two hysteretic components in parallel with the conventional stiffness and damping elements. The two hysteretic components are the MRE and MRF components. They are either a Bouc-Wen, Modified Dahl, or LuGre Friction components, adding up to 9 generalized models. Then, the parameters of each model are estimated using the Trust-region-reflective algorithm. The most precise model is selected by

Table 1

Material Properties of the silicone rubber and CIPs ("Elite Double 32 Fast, 2023"), ("Carbonyl iron powder, 2023").

Materials	Properties	
Silicone rubber	Type	Elite Double 32 Fast
	Density [g/cm^3]	1.06
	Detail reproduction [μm]	2
	Mixing ration	1:1
	Setting time [min:s]	10:00
	Hardness	22
	Tear resistance [N/mm^2]	5
	Elastic recovery [%]	99.95%
CIPs	Type	SQ-I
	Density [g/cm^3]	7.89
	Particle size [μm]	4.5
	Coating	SiO_2
	Permeability [N/mm^2]	10

comparing the minimum root mean square error between the model-predicted results and the testing data. The significance and physical meaning of each parameter is then studied. Finally, the relationship between the model parameters, excitation frequency, and current level are studied and expressed as third-order polynomials to contribute to a field-dependent model. An overview of the methodology of this work is presented in Fig. 1.

The paper is organized as follows. Section 2 presents the modelling and testing of the hybrid MRE-based isolator. Section 3 presents the hysteresis models and the parameter identification process. Section 4 presents the frequency and field-dependent modelling of the parameters. The summary and concluding remarks are highlighted in Section 5.

2. Methodology

2.1. Materials

The materials used in this process are silicone rubber, magnetic particles, and MR fluid. Zhermack's Elite Double 32 Fast silicone rubber is used as the elastomer matrix due to its many advantages. Its short working time (10–15 min) helps minimize the effect of magnetic particle sedimentation during the curing process, and its high fluidity allows easy mixing without vacuum conditions. This type also offers high dimensional stability over time and high elastic recovery. The magnetic particles used in this study are carbonyl iron particles (CIPs), which are formed through the thermal decomposition of iron pentacarbonyl. These particles are suitable for use in the fabrication of MREs due to their easy magnetization, high saturation and demagnetization characteristics. The type of CIPs used in the study is SQ-I, developed by BASF and has high magnetic saturation and permeability. It is also coated with silicone dioxide to enhance compatibility with the elastomer matrix and prevent sedimentation (Dang et al., 2010). The magnetic particles are poly-disperse with a varying size distribution, which helps enhance the material's MR effect (Jaafar et al., 2021), (Stepanov et al., 2007). A 10% volume fraction of CIPs is used in the MRE mixture. This amount is chosen because it allows for sufficient magnetization while maintaining passive stiffness. The material properties of the silicone rubber and CIPs are summarized in Table 1. The incorporation of magnetic fillers significantly impacts the stiffness and hardness of MRE samples. Soft MRE samples exhibit superior elastic behavior and are capable of isolating more vibrations. However, if the rubber material is excessively soft, it may not be able to fully recover from deformations fully, thereby reducing the effectiveness of vibration isolation. To strike a balance between magnetization and passive stiffness, CIPs are added with a 10% volume fraction. The magnetic particles used in the study are poly-disperse, indicating a variation in their particle size distribution. This is crucial in achieving a better MR effect due to the packing of particles in chain-like aggregates and the increased magnetic dipole interaction with adjacent particles.

A customized casting mold is used to create the hybrid MRE samples. The mold is fabricated using 3D printing and consists of three plates. The lower and upper plates have central tips that hold Styrofoam pieces, while the middle plate determines the overall length of the sample. The
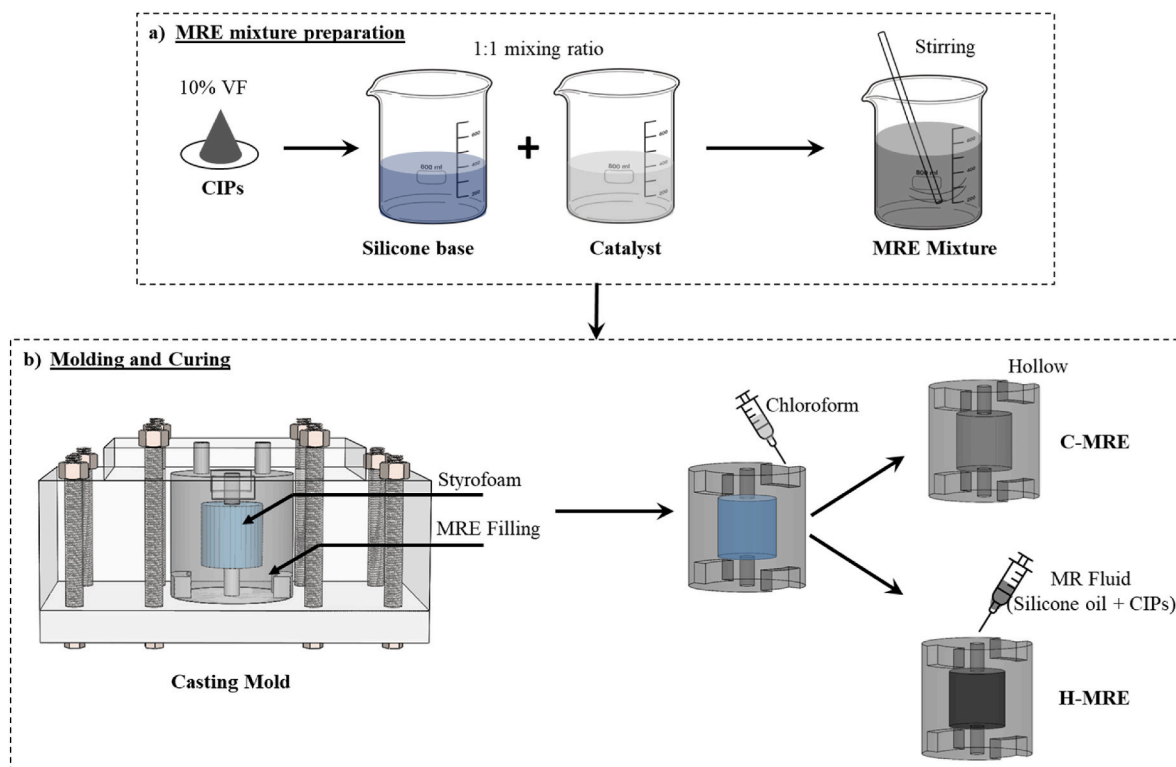

Fig. 2. Fabrication of the conventional and hybrid MREs. (C-MRE & H-MRE): (a) MRE mixture preparation, (b) Molding and curing.

Table 2
Types and names of the fabricated samples.

SN.	Type	Name	Matrix 1	Matrix 2	Magnetic particles
1	Conventional	C-MRE	MRE	None	CIPs
2	Hybrid	H-MRE	MRE	MR fluid	CIPs

mold can be easily modified to create MRE samples of different lengths by changing the height of the middle plate. The lower and upper plates of the mold have jaws that will hold the hybrid MRE samples in place within the flexible jaw coupling.

2.2. Fabrication process

The fabrication process of hybrid MRE material is performed via direct molding and involves four main steps. The first step involves preparing the MRE mixture. The second step involves creating a casting mold using 3D printing and assembling it. The third step involves molding and curing the MRE mixture. The final step involves injecting a viscous MR fluid into the MRE cavity. The silicone base is mixed with CIPs and stirred properly; the silicone catalyst is added with a 1:1 mixing ratio to create the MRE mixture, as shown in Fig. 2(a). After adequate stirring, the mixture is poured into the mold containing the piece of Styrofoam. The mold is then covered, and any excess liquid can flow through the top risers. After the sample has cured, chloroform is used to dissolve the Styrofoam and leave a cavity inside the elastomer, as shown in Fig. 2(b), which is then filled with MR fluid creating the hybrid sample, referred to as H-MRE. An additional MRE sample, referred to as the C-MRE, is made using the same process as the other samples but without adding any fluid. The details of the fabricated samples are presented in Table 2.
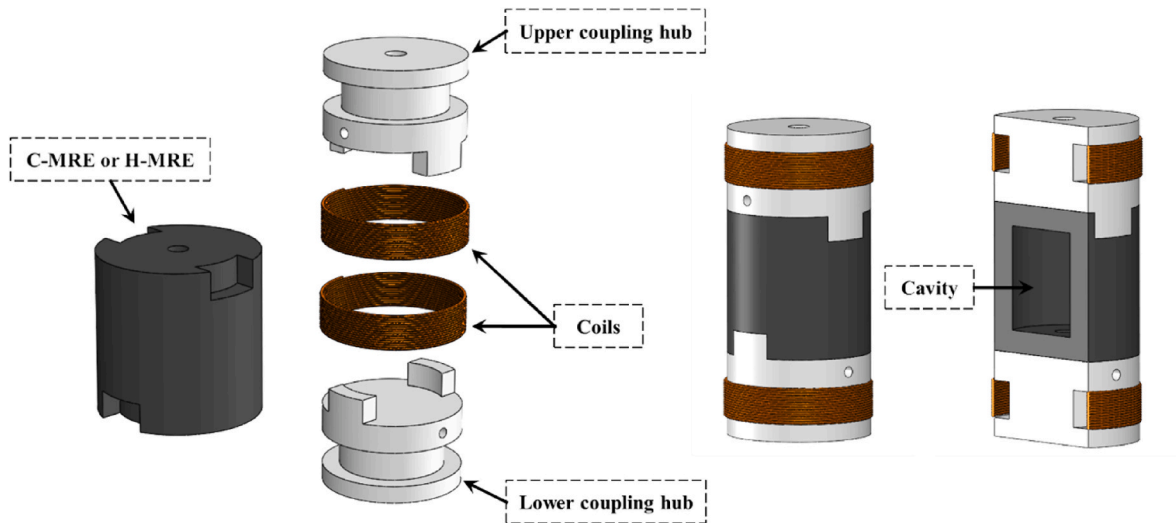

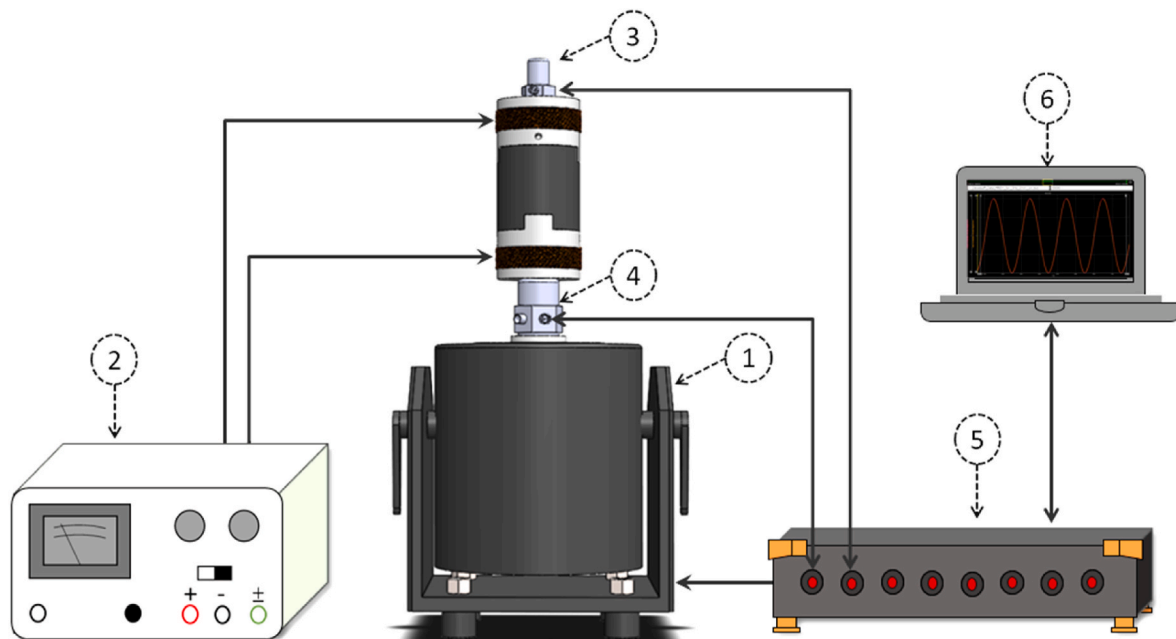**Fig. 3.** Design and assembly of the semi-active isolator.

Fig. 4. Schematic representation of the experimental setup: (1) vibration shaker, (2) power supply, (3) accelerometer, (4)) impedance sensor, (5) data acquisition system, (6) computer with signal analyzing software.

Table 3
Testing parameters and details.

Variable	Value
Excitation	Sinusoidal wave
Current (A)	0, 1, 2, and 3
Frequency (Hz)	3, 5, 7, and 9
Amplitude (mm)	2

Table 4
Details of the proposed model.

Model No.	Hysterestic Component				Total No. of Parameters
	MRE		MRF		
	Type	No. of parameters	Type	No. of parameters	
1	Bouc-Wen	6	Bouc-Wen	6	12
2	Bouc-Wen	6	Modified-Dahl	5	11
3	Bouc-Wen	6	LuGre friction	5	11
4	Modified-Dahl	5	Bouc-Wen	6	11
5	Modified-Dahl	5	Modified-Dahl	5	10
6	Modified-Dahl	5	LuGre friction	5	10
7	LuGre friction	5	Bouc-Wen	6	11
8	LuGre friction	5	Modified-Dahl	5	10
9	LuGre friction	5	LuGre friction	5	10

2.3. Semi-active isolator design and assembly

The hybrid MRE-based semi-active isolator is a flexible jaw coupling comprising four main parts: the top and bottom coupling hubs, the coils, and the H-MRE layer, as shown in Fig. 3. The proposed coupling can be used for vibration base isolation. The coupling is designed to allow coils to wind around the grooved section of the coupling hubs. Hence, the coupling can act as an electromagnet when current is supplied to the coils, creating a magnetic field in the MRE layer. Moreover, the coupling is designed so that the magnetic polarity of the electromagnetic coupling causes the magnetic flux to pass through the MRE layer. The intensity of the magnetic field created by the electromagnetic coils is measured using a Tesla meter at various current levels. The measurement is taken on the surface of the jaw connection between the MRE layer and the coupling hub, which is where the maximum magnetic flux is concentrated. It is observed that the magnetic flux within the electromagnetic coils increases with the current. These measurements demonstrate that the MRE layer is exposed to sufficient magnetic flux to achieve the desired MR effect.

2.4. Experimental setup and testing

The developed C-MRE and H-MRE based semi-active isolators are tested through a series of longitudinal vibration tests with harmonic base excitations. The tests are conducted to evaluate and characterize the proposed semi-active isolators. The test data are then used to perform the parameter identification of the proposed parametric models. The tests are conducted by employing the experimental setup shown in Fig. 4. A permanent magnet vibration shaker (DS-PM-100) from Dewesoft® is used as the excitation source for the tests. This shaker has an integrated power amplifier and is controlled by a data acquisition system. The semi-active isolator is placed between an impedance sensor and an accelerometer. The impedance sensor is attached to the shaker's excitation port to measure the input force and acceleration, while the

accelerometer measures the output acceleration from the isolator. The tests are controlled, and the data are recorded by a Dewesoft Sirius data acquisition system (DAQ). The vibration shaker is connected to an output channel of the DAQ. Harmonic base excitations are performed using sinusoidal wave inputs with fixed frequencies. The sensors are connected to the input channels of the DAQ, and the output displacement responses are recorded and analyzed in real-time using an embedded dynamic signal analyzer. The tests are performed with different excitation frequencies (3, 5, 7, and 9 Hz) and current levels (0–3 A). The testing parameters and details are summarized in Table 3.

3. Parametric modelling

3.1. Approach

Modeling the behavior of an H-MRE semi-active isolator, which uses MRE and MRF, can be difficult because it requires accurately representing the nonlinear and hysteretic relationship between force and displacement for both the MRE and MRF components. This is necessary to capture the isolator's behavior accurately. Generally, the hybrid material could be prepared in two different methods. Method 1: Mixing MRE (silicone base + CIP + catalyst) and MRF (silicone oil + CIP) together during curing process. In this preparation method, MRF will be trapped and distributed throughout MRE as tiny particles. The dynamic performance and behavior of such samples are not dominated by the individual behavior of MRE or MRF. As such, this sample may be described or approximated using only a single hysteresis model, and optimization can be done for that single model. Method 2: Encapsulating a larger amount of MRF inside MRE. Unlike method 1 above, in this method, a larger amount of MRF is placed/encapsulated inside a hollow MRE. The dynamic behavior of this sample is largely dominated by the individual behavior of MRE and MRF, and the sample's dynamic performance cannot be diluted by using only a single hysteresis model. Hence, it is required to use suitable model for each MRE and MRF separately for samples prepared via method 2.

The proposed model consists of two hysteretic components, in parallel with a Kelvin-Voigt model, which describes the solid-material properties such as stiffness and damping. The Voigt elements consist of a parallel spring element and a damping element. Each of the MRE and MRF compartments is represented by one of the hysteretic components parallel to the other. These components are used to reproduce the hysteresis loops of such materials, allowing the model to capture the isolator's unique behaviour accurately.
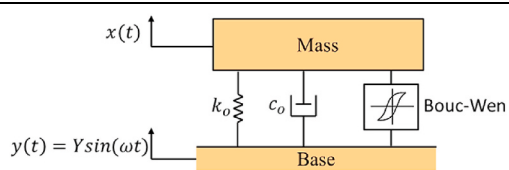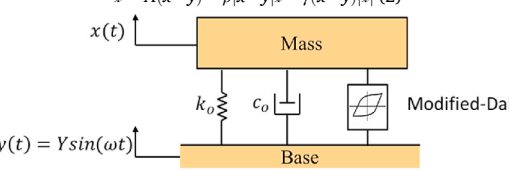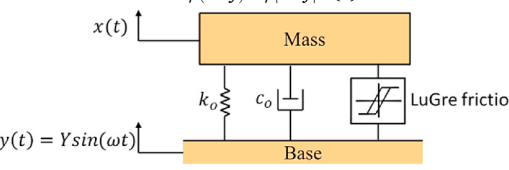
To create a general model that accurately represents the behavior MRE and MRF compartments, multiple models are developed that incorporate various combinations of Bouc-Wen, Modified Dahl, and LuGre Friction hysteretic components. This results in a total of nine models. The model with the lowest root means square error between the testing data and predicted results is selected. This approach is used to determine the optimal combination of hysteretic components for accurately modeling the response of isolators that utilize two different magnetorheological materials. A summary and description of the models are presented in Table 4. An overview of the phenomenological model employed in this study is given in the subsequent subsection. The schematics and the expressions of the hysteresis forces and nonlinear variables of the models are summarized in Table 5.

3.2. Overview of the hysteresis models

3.2.1. Bouc-Wen model
The Bouc-Wen model consists of two components in parallel: one representing the solid material behavior using a Voigt model and the other representing hysteresis using a Bouc-Wen model (Yang et al., 2013). The hysteresis force of this nonlinear system is formulated as in Eq. (1). In this model, x and $\dot{x}$ represent the displacement and velocity, respectively, of the magnetorheological elastomer device, while y and $\dot{y}$

Table 5
Schematics and the expressions of the models' hysteresis forces and nonlinear variables.

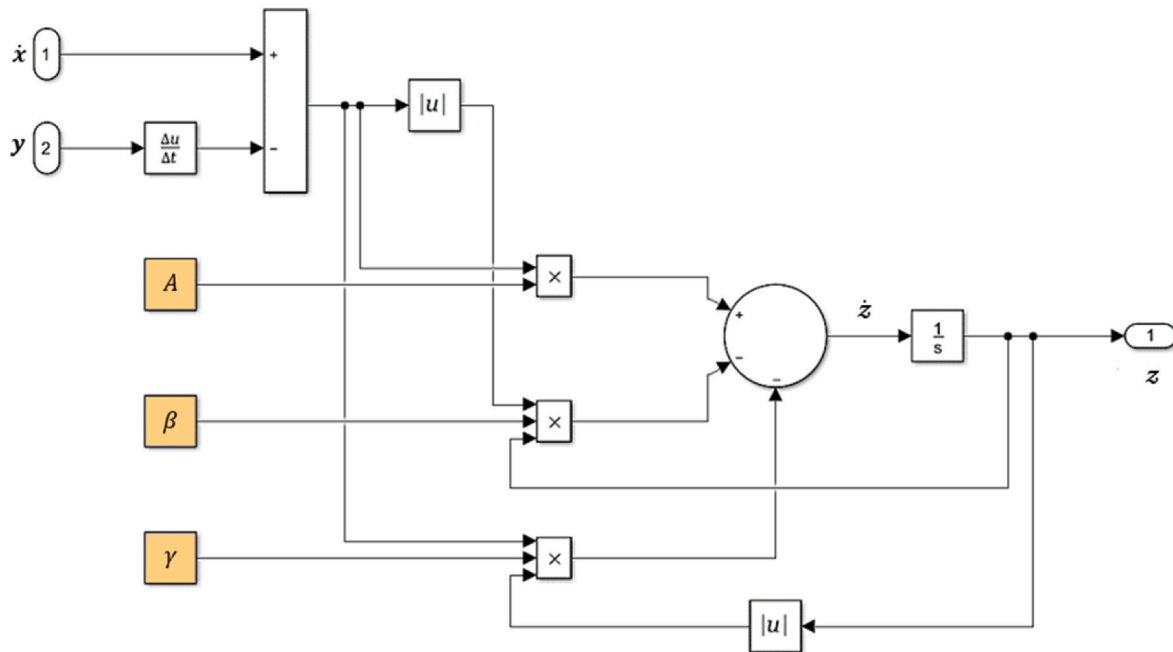| Model	Schematic - Expressions	Parameters
Bouc-Wen	$F = \alpha k_o(x-y) + (1-\alpha)k_o z + c_o(\dot{x}-\dot{y})$ (1) $\dot{z} = A(\dot{x}-\dot{y}) - \beta\|\dot{x}-\dot{y}\|z - \gamma(\dot{x}-\dot{y})\|z\|$ (2)	$k_o, c_o, \alpha, A, \beta, \gamma$
Modified Dahl	$F = k_o(x-y) + c_o(\dot{x}-\dot{y}) + \alpha z - f_o$ (3) $\dot{z} = \rho(\dot{x}-\dot{y}) - \rho\|\dot{x}-\dot{y}\|z$ (4)	$k_o, c_o, \alpha, \rho, f_o$
LuGre friction	$F = k_o(x-y) + c_o(\dot{x}-\dot{y}) + \frac{\beta}{\alpha}z + \frac{\varepsilon}{\alpha}\dot{z}$ (5) $\dot{z} = \alpha(\dot{x}-\dot{y}) - \alpha\|\dot{x}-\dot{y}\|z$ (6)	$k_o, c_o, \alpha, \beta, \varepsilon$

Fig. 5. Simulink representation of the Bouc-Wen model hysteresis: $\dot{z} = A(\dot{x} - \dot{y}) - \beta\|\dot{x} - \dot{y}\|z - \gamma(\dot{x} - \dot{y})\|z\|$.

represent the displacement and velocity, respectively, of the base excitation. The stiffness and viscous coefficients of the system are represented by k_o and c_o, respectively. The parameter α, which ranges from 0 to 1, scales the model. The mathematical expression of $\dot{z}$ is given in Eq. (2), where z is an intermediate variable that represents the device's displacement history, and $\dot{z}$ is the derivative of z with respect to time. The parameters A, β, γ control the size and shape of the hysteretic loop. The Bouc-Wen model of hysteresis is depicted in a graphical representation using Simulink in Fig. 5.

3.2.2. Modified-Dahl model

The Dahl model was developed initially to simulate control systems with friction. It can be used to model nonlinear force-displacement loops through a differential equation. Zhou et al. (2006) proposed a modified Dahl model for MR dampers that is simple and effective. In the modified Dahl model, the Dahl hysteresis operator is used instead of the Bouc-Wen hysteresis operator to simulate the Coulomb force because it requires fewer parameters to be determined and effectively captures the force-velocity relationship at low velocities. The hysteresis force and evolutionary variable of this model are represented by Eq. (3) and Eq.
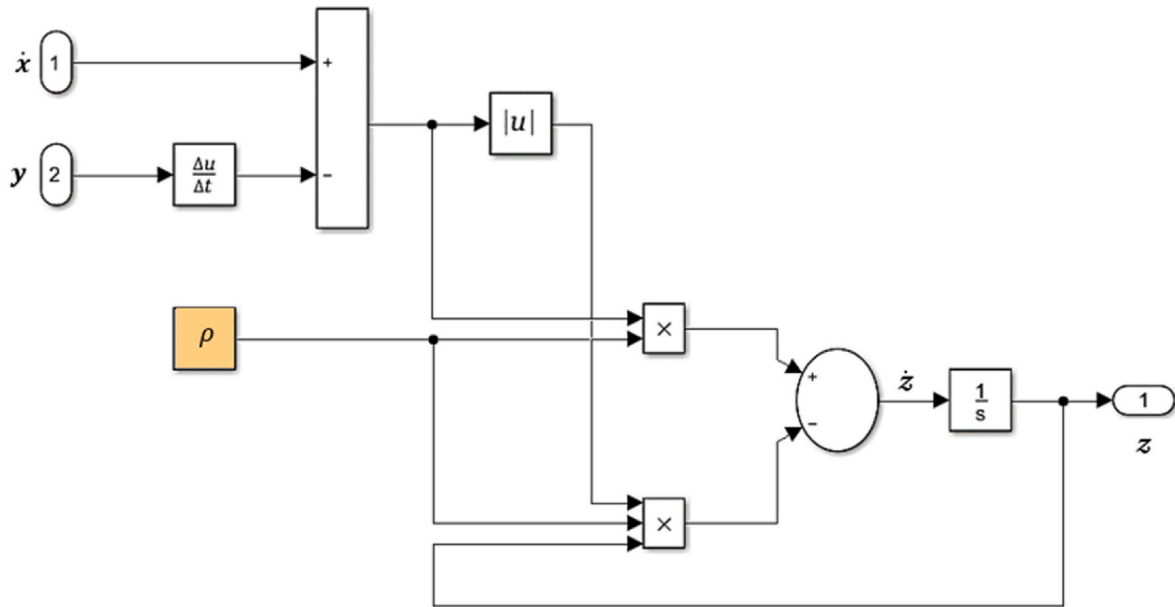
Fig. 6. Simulink representation of the Modified Dahl model hysteresis: $\dot{z} = \rho(\dot{x} - \dot{y}) - \rho|\dot{x} - \dot{y}|\,z$.
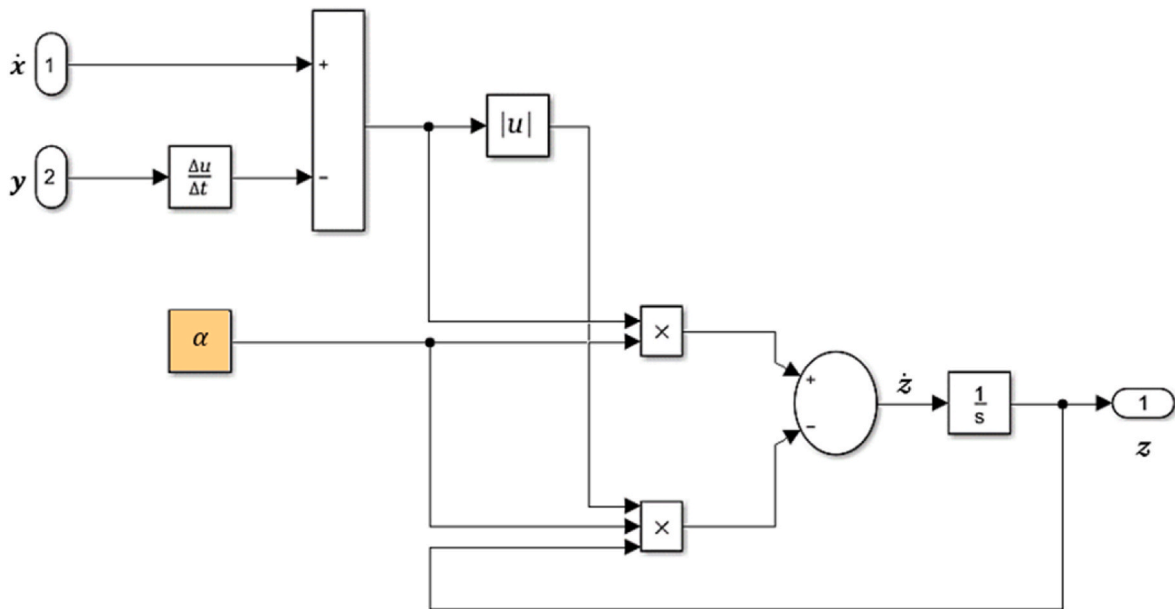

Fig. 7. Simulink representation of the LuGre friction model hysteresis: $\dot{z} = \alpha(\dot{x} - \dot{y}) - \alpha|\dot{x} - \dot{y}|\,z$.

(4), respectively, where c_o and k_o represent the viscous and stiffness coefficients, respectively. The parameter α scales the shape of the hysteresis loops, while z is an intermediate variable. The parameter ρ is related to the stiffness of the system. The modified Dahl hysteresis model is depicted in a graphical representation using Simulink in Fig. 6.

3.2.3. LuGre friction model

The LuGre friction model, which is an extension of the Dahl model, was designed to describe the friction dynamics of MREs. It has been used to model the dynamic behavior of an MRE isolator (Yu et al., 2015). The model consists of a viscous dashpot, a linear spring element, and a LuGre friction component. This model's hysteresis force and evolutionary variable are represented by Eq. (5) and Eq. (6), respectively. In the LuGre model, c_o and k_o represent the viscous and stiffness coefficients, respectively. The parameters α, β, and ε control the size and shape of the

hysteresis loops, while z is an evolutionary variable. The hysteresis of LuGre friction model is depicted in a graphical representation using Simulink in Fig. 7.

3.3. Optimization algorithm

To evaluate the proposed models' effectiveness in predicting the semi-active isolator's response with an H-MRE sample, an optimization algorithm that combines least-squares and Trust-region-reflective methods were used to find the optimal values for the set of parameters of the respective models. This optimization algorithm was implemented in MATLAB. The trust region reflective algorithm is an optimization method that involves minimizing an objective function, denoted as $g(x)$, by constructing and minimizing a simpler approximation function, $p(x)$, within a specified region around the current point, called the trust
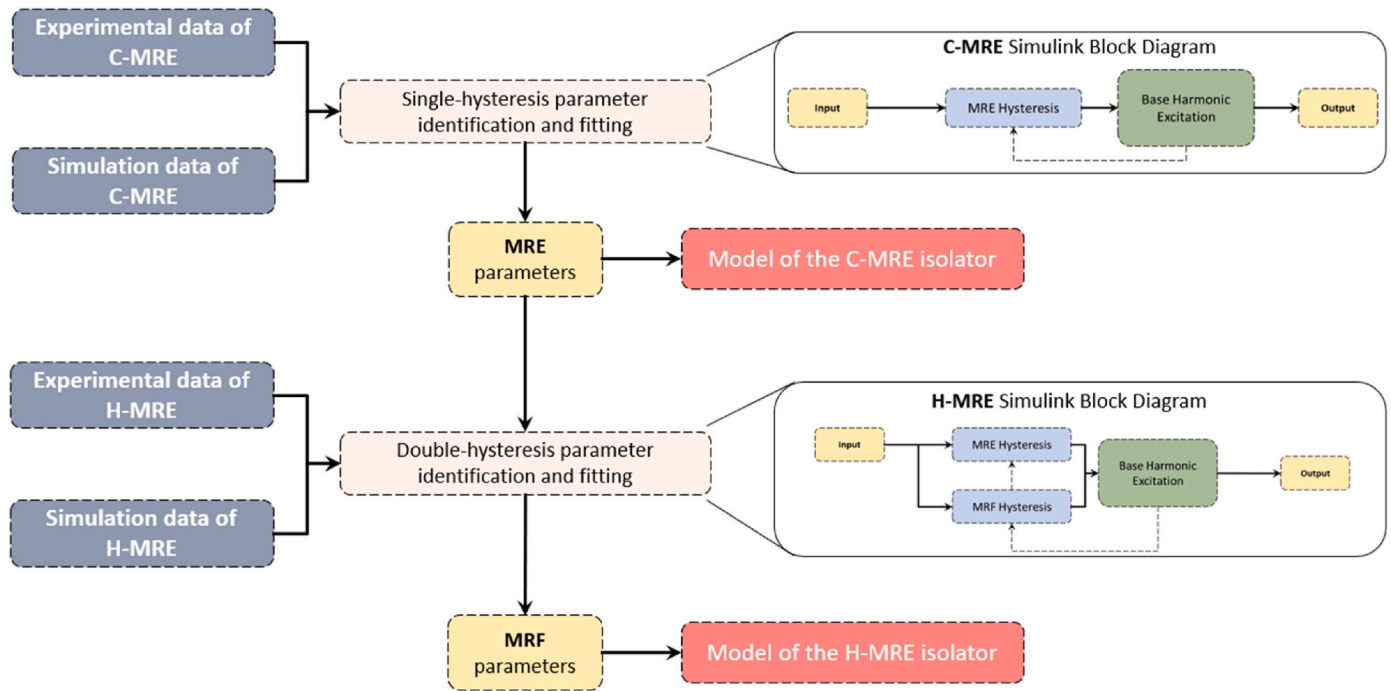
Fig. 8. Overview of the parameter identification process.

Table 6
RMSE between the actual and model-predicted responses for all models.

Model Combinations		MRF component		
		Bouc-Wen	Modified-Dahl	LuGre friction
MRE component	Bouc-Wen	1.37	1.12	0.996
	Modified-Dahl	1.54	1.08	1.02
	LuGre friction	0.963	0.993	0.995

Table 7
Optimal values of the parameters identified using a combination of LuGre friction and Bouc-Wen models. (5Hz – 1A).

MRE parameters using LuGre friction				
k_{o_e}	c_{o_e}	α_e	β_e	ε_e
137.5221 (N/mm)	5.4623 (N.s/mm)	0.5734	0.0841	0.0736

MRF parameters using Bouc-Wen					
k_{o_f}	c_{o_f}	α_f	A_f	β_f	γ_f
8.8835 (N/mm)	16.8654 (N.s/mm)	0.3907	0.3933	0.5386	−0.3623

region. The optimization variables in the trust region reflective algorithm are the model parameters, and the goal is to find the values of these parameters that minimize the objective function. The objective herein is to minimize the root mean square, as indicated by:

$$J = \sum_{i=1}^{N} \sqrt{\frac{(PR_i - AR_i)^2}{N}} \tag{7}$$

where N is the number of input–output pairs in each loop; PR indicates the model-predicted response; and AR is the experimentally obtained response.

The proposed models have many parameters because they include two hysteretic components, one for the MRE compartment and one for the MRF compartment. Therefore, the parameter identification process is conducted over two stages. In the first stage of the parameters identification, three different Simulink models of a C-MRE semi-active isolator are used, each representing a different type of the hysteretic component (Bouc-Wen, Modified-Dahl, or LuGre friction) for the MRE compartment. The models are simulated, and the responses of these models are optimized to fit C-MRE experimental data of a 5 Hz frequency, 1 A of current, and 2 mm of amplitude. As a result, the optimized parameters for the MRE component in each of the three models are obtained.

In the second parameter identification stage, the MRF component parameters are identified using nine different Simulink models of a H-MRE semi-active isolator. Each model includes two hysteretic components that are combinations of Bouc-Wen, Modified-Dahl, or LuGre friction models, where the parameters for the MRE hysteretic component are obtained from the first stage of the simulation. The models are then simulated, and the parameters for the MRF component are obtained by optimizing the models to fit the experimental data for the H-MRE semi-active isolator. An overview of the parameter identification process performed in this study is presented in Fig. 8.

For the Simulink simulations, a variable step solver with an automatic solver is selected to improve the accuracy and efficiency of the simulation. A variable step solver allows the solver to adjust the time step size at each time point based on the system's simulated characteristics. This can result in a more accurate simulation because the solver can take smaller time steps in regions of the model where the behavior changes rapidly and larger time steps where the behavior is relatively constant. Using an automatic solver selection option allows Simulink to choose the best solver for the system based on the model's characteristics and the simulation's requirements. This can further improve the accuracy and efficiency of the simulation because the solver can select a solver that is well-suited to the characteristics of the model.

4. Parameters estimation results

The predicted responses of the proposed models are validated against the actual response. It is observed that the nine hysteresis models can
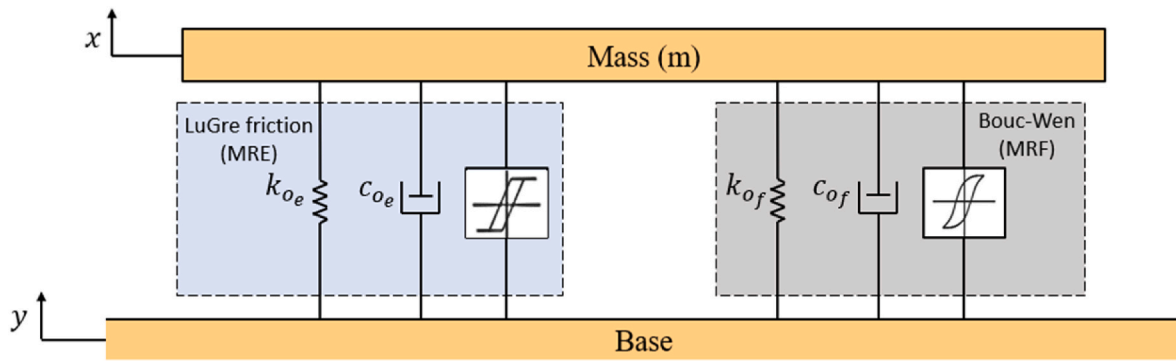
Fig. 9. Schematic of the semi-active base isolator using the H-MRE material with LuGre friction hysteresis components for MRE and Bouc-Wen for MRF hysteresis in parallel. The structure includes the mass (*m*), the output displacement (*x*), and the harmonic excitation input at the base (*y*).
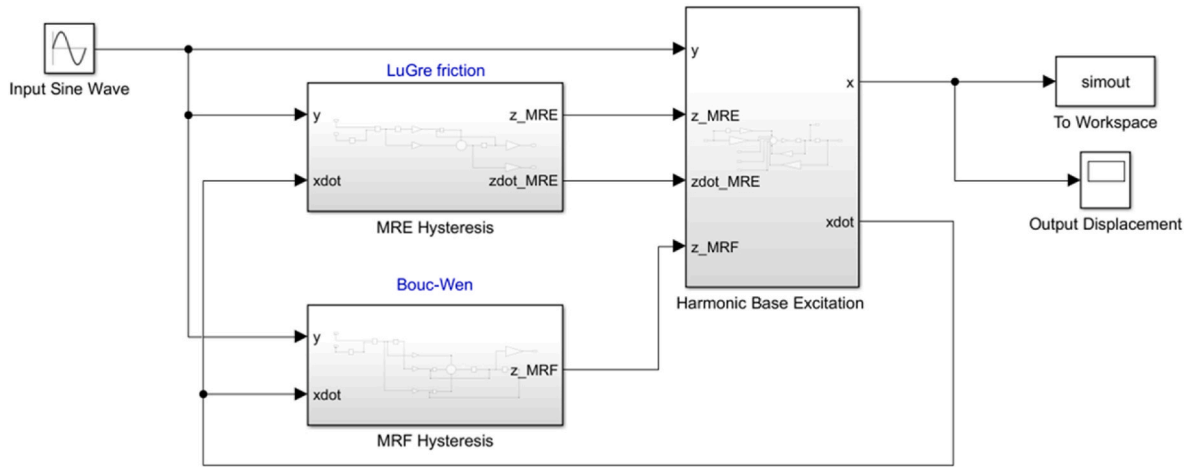

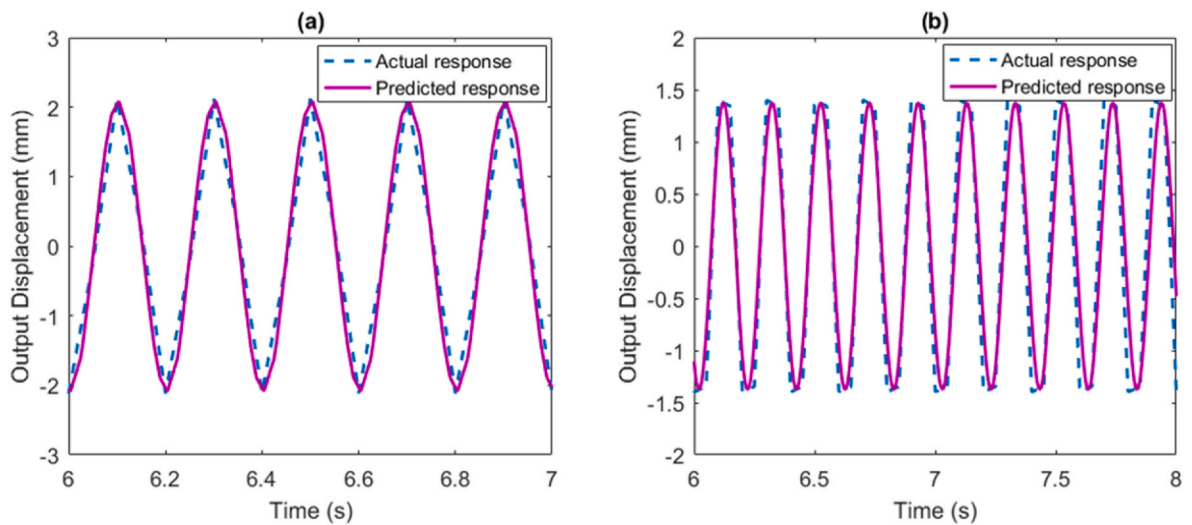**Fig. 10.** Simulink block diagram of the proposed model.

Fig. 11. Actual and model-predicted output displacement response of (a) the C-MRE semi-active base isolator and (b) H-MRE semi-active base isolator. Results are obtained at 5 Hz frequency, 1 A current and 2 mm amplitude.

predict the response of the H-MRE semi-active isolator. It is also observed that the LuGre friction and Modified-Dahl models have similar behaviors because the LuGre model was developed as a variation of the Dahl model, to describe the behavior of friction in MREs in more detail. The LuGre model incorporates additional terms that consider the effects of slip velocity and amplitude on the frictional force. As a result, the responses of the LuGre model and the Dahl model can be very similar in some cases. However, the LuGre model can be more accurate in capturing the friction dynamics of MREs, especially at high slip velocities and/or amplitudes. Additionally, it is observed that the Bouc-wen
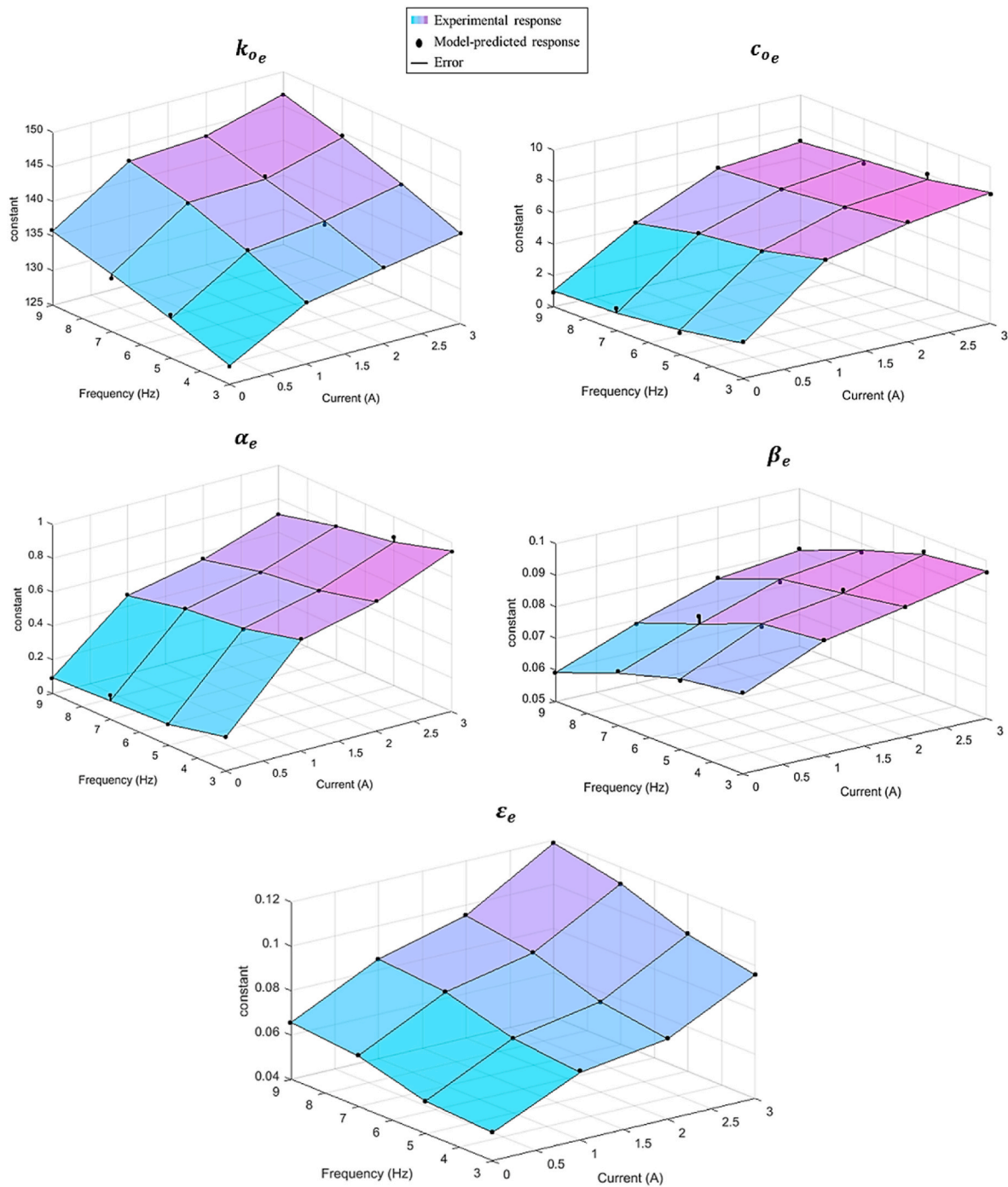
Fig. 12. Parameters value of the LuGre friction model of the MRE component as a function of current and frequency.

model can provide more accurate predictions of the dynamic response of MRFs when compared to other models, especially in capturing the hysteretic behavior of MR fluids under cyclic loading conditions. The best combination of hysteresis models to represent the hybrid isolator's performance is determined by computing the root mean square error (RMSE) between the actual and predicted responses of the models. The findings of the RMSE calculations are presented in Table 6.

Generally, the proposed model combinations exhibit an excellent capability in predicting the isolator response. However, upon analyzing the errors, it appears that using a combination of the LuGre friction model for the MRE component and the Bouc-Wen model for the MRF component seems to be the most effective in replicating the performance of the H-MRE isolator. The optimal values for the parameters that have

been determined using this model are summarized in Table 7. The subscripts " e " and " f " refer to the parameters of the MRE and MRF components, respectively.

The proposed model for the H-MRE isolator is modeled as a single-degree-of-freedom structure with a hysteretic property, as shown in Fig. 9. The following equation of motion can describe the model behavior.

$$m\ddot{x} + F_{mre} + F_{mrf} = 0 \qquad (8)$$

The hysteresis forces F_{mre} and F_{mrf} are described using Eq. (1) and (5) as follows:
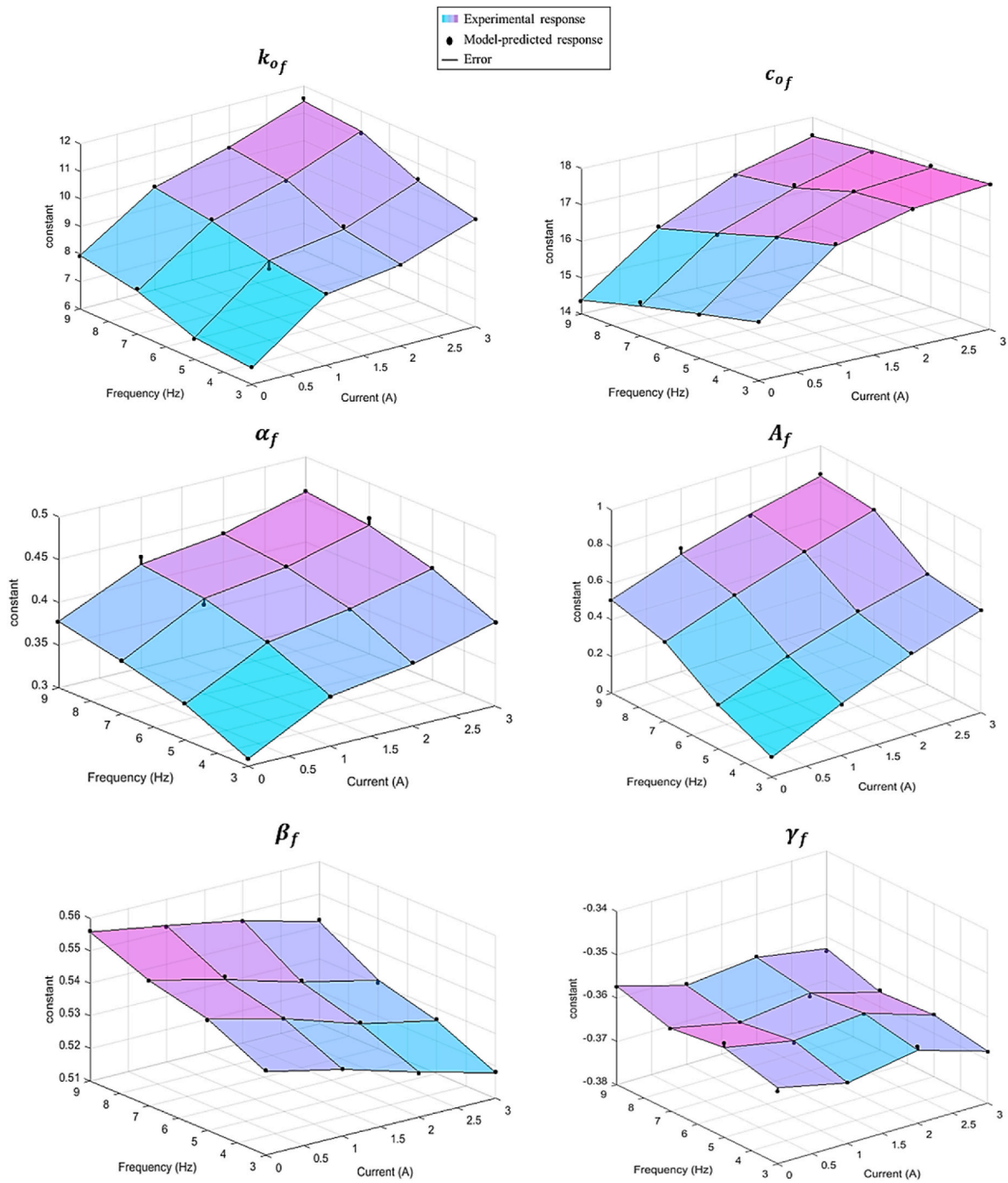
Fig. 13. Parameters value of the Bouc-Wen model of the MRF component as a function of current and frequency.

$$F_{mre} = k_{o_e} x_r + c_{o_e} \dot{x}_r + \frac{\beta_e}{\alpha_e} z_e + \frac{\varepsilon_e}{\alpha_e} \dot{z}_e \qquad (9)$$

$$F_{mrf} = \alpha_f k_{o_f} x_r + c_o \dot{x}_r + (1 - \alpha_f) k_{o_f} z_f \qquad (10)$$

The variables $\dot{z}_e$ and $\dot{z}_f$ are defined as in Eq. (2) and (6), respectively. Hence, Eq. (1) can be rewritten as:

$$\ddot{x} = a_1 x_r + a_2 \dot{x}_r + \varphi \qquad (11)$$

In Eq. (11), a_1 and a_2 are system parameters, $x_r = x - y$ is the relative displacement, $\dot{x}_r = \dot{x} - \dot{y}$ is the relative velocity, and φ represents the hysteresis components of the structure. These parameters are defined as:

$$a_1 = -\frac{k_{oe} + \alpha_f k_{of}}{m}, a_2 = -\frac{c_{oe} + c_{of}}{m}, \text{and,} \varphi =$$

$$-\frac{1}{m} \left[\frac{\beta_e}{\alpha_e} z_e + \frac{\varepsilon_e}{\alpha_e} \dot{z}_e + (1 - \alpha_f) k_{o_f} z_f \right]$$

The Simulink block diagram of the model is presented in Fig. 10. The model consists of two hysteresis subsystems for the MRE and MRF components, which are then used along the input sine wave for the harmonic base excitation in Eq (11). The MRE portion of the system is first characterized by utilizing the LuGre friction subsystem to simulate the dynamic behavior of the C-MRE isolator. The remaining parameters of the MRF component are then determined by incorporating the Bouc-Wen subsystem into the model, which simulates the proposed H-MRE

Table 8

Proposed polynomial equations of the model parameters.

MRE parameters using LuGre friction		
k_{o_e}	$k_{o_e} = 121.5 + 12.03\,i + 2.317\,f - 6.434\,i^2 + 0.01855\,if - 0.1055f^2 + 1.197\,i^3 - 0.0006567\,i^2f - 0.000368f^2 + 0.002755\,f^3$	(12)
c_{o_e}	$c_{o_e} = 4.684 + 5.456\,i - 1.142\,f - 1.715\,i^2 - 0.03021\,if + 0.1358\,f^2 + 0.1688\,i^3 + 0.02928\,i^2f - 0.00356\,if^2 - 0.006221\,f^3$	(13)
α_e	$\alpha_e = 0.5769 + 0.7673\,i - 0.2025\,f - 0.365\,i^2 - 0.003164\,if + 0.03015f^2 + 0.06369\,i^3 + 0.002188\,i^2f - 0.0008584\,if^2 - 0.001522\,f^3$	(14)
β_e	$\beta_e = 0.07124 + 0.01201\,i + 0.003623\,f - 0.003043\,i^2 + 0.0002951\,if - 0.0008185f^2 + 0.0004114i^3$	(15)
ε_e	$\varepsilon_e = 0.08315 + 0.03059\,i - 0.02031\,f - 0.01829i^2 + 0.0003426\,if + 0.004058\,f^2 + 0.004079\,i^3 - 0.0002244\,f^3$	(16)
MRF parameters using Bouc-Wen		
k_{o_f}	$k_{o_f} = 9.413 + 2.947\,i - 1.832\,f - 1.59i^2 + 0.09954\,if + 0.359f^2 + 0.2885\,i^3 + 0.01071\,i^2f - 0.009506\,if^2 - 0.01933\,f^3$	(17)
c_{o_f}	$c_{o_f} = 15.58 + 2.302\,i + 0.164\,f - 0.7492\,i^2 - 0.03222\,if - 0.06131\,f^2 + 0.06726\,i^3 + 0.02455\,i^2f + 0.0001088\,if^2 + 0.003126\,f^3$	(18)
α_f	$\alpha_f = 0.2296 + 0.08296\,i + 0.0334\,f - 0.04091\,i^2 + 0.000274\,if - 0.002571\,f^2 + 0.007471\,i^3 + 0.0002635\,i^2f - 0.0001205\,if^2$	(19)
A_f	$A_f = 0.5696 + 0.2462\,i - 0.351\,f - 0.0222\,i^2 - 0.01937\,if + 0.07976\,f^2 + 0.001319\,i^3 + 0.0008107\,i^2f + 0.0008792\,if^2 - 0.004614\,f^3$	(20)
β_f	$\beta_f = 0.4976 - 0.003662\,i + 0.02049\,f - 0.001185\,i^2 - 0.0005895\,if - 0.003077\,f^2 + 0.0003183\,i^3 + 0.000169f^3$	(21)
γ_f	$\gamma_f = -0.3957 - 0.007368\,i + 0.01935\,f + 0.008168\,i^2 - 0.0007284\,if - 0.003322\,f^2 - 0.002027\,i^3 + 0.0001311\,i^2f + 0.0001828\,f^3$	(22)

isolator. The performance of the C-MRE isolator is compared to the predicted results and shown in Fig. 11(a), while the response of the H-MRE isolator is illustrated in Fig. 11(b).

5. Parameters identification at various loading conditions

To further validate the selected model's ability to represent the behavior of the H-MRE isolator, additional sets of comparisons are made between the predicted and measured data for various loading conditions. Additional simulations are performed, and the new estimations are optimized to fit the experimental data, of 3, 7 and 9 Hz frequencies and current levels ranging from 0 to 3 A with a 2 mm amplitude. The optimal values of both the LuGre friction and Bouc-Wen models are obtained at various frequencies and current levels. The variation of the estimated parameters of both models with respect to the frequency and current are presented in Figs. 12 and 13.

The results indicate that the effectiveness of an H-MRE semi-active isolator is influenced by the frequency at which it is excited and the strength of the magnetic field applied to it. Previous studies have pointed out that the performance is also related to the amplitude of the loading the isolator experiences (Yu et al., 2016). Therefore, the device's magnetic field dependence can be visualized by examining the relationship between the model parameters and the loading conditions provided in this paper.

It can be observed that the parameters of the LuGre friction model that simulate the hysteresis of the MRE component are affected by both the excitation frequency and the applied current. However, the degree to which these parameters are sensitive to the changes in loading conditions varies among them. The parameter, k_{o_e}, is current dependent at different frequencies. As the current increases, k_{o_e}, increases as well due to the alignment and interaction of the magnetic particles. Similarly, as the frequency of excitation increases, k_{o_e}, increases due to the deformation of the matrix, leading to increased entanglement of the particles (; ; Ali et al., 2022). The parameter, c_{o_e}, is also current dependent, however, is less sensitive to the frequency variations. As the current increases, c_o, increases due to the growing friction between the magnetic particles, leading to higher energy dissipations. It is further observed that the hysteresis-related parameters, such as α_e and ε_e are more sensitive to the current variations than the frequency variations. The parameter, β_e, demonstrated the least level of responsiveness to changes in both current and frequency. These findings can help design semi-active isolators that use the LuGre friction model to identify MRE hysteresis.

Among all the parameters of the Bouc-Wen model that simulate the hysteretic response of the MRF components, $k_{o_f}, c_{o_f}, \alpha_f$ and A_f, exhibited a strong field-dependance at different excitation frequencies. However, the parameter, c_{o_f}, is less sensitive to the change in frequency. The

stiffness parameter, k_{o_f}, of the MRF component increase with the applied current due to the increased inter-particle connections between the magnetic particles that form a chain-like structure when subjected to a magnetic field. Similarly, the viscous parameter, c_{o_f}, increases with the current, as the interactions and friction of the magnetic particles lead to more energy dissipation. It is observed that the parameter, α_f, is sensitive to the loading conditions, as it is affected by the excitation frequency and the input current. However, it increases at a higher rate when the input current increases and becomes less dependent on the field as the frequency increases. The parameters β_f, and γ_f, do not vary significantly with changes in frequency and current, with the latter not showing a specific pattern of variation. β_f and γ_f have an effect the size and shape of the hysteresis loop, however, these parameters lack physical interpretation and affect the system response in ambiguous manner, hence are not field-dependent (Yang et al., 2013), (Yu, Li, Li, Li, Li, Wang). The values of these nonlinear parameters are typically determined through a combination of experimental data and theoretical analyses, and they are assumed to be constant for a given application. This is because they represent the intrinsic properties of the model and are not affected by the specific properties of the structural system being modeled.

The relationship between each parameter and the frequency and current are described as polynomial equations. This is done through curve fitting the predicted response on the experimental measurements. The curve fitting is performed using the MATLAB curve fitting toolbox. The toolbox uses optimization techniques like least squares to fit the models. The polynomial order that provides the best fit, in terms of the highest accuracy and lowest error, is determined to be the third order. It is observed that using third-order polynomials allows for an efficient and accurate fitting of the model in a short computational time. The proposed polynomial equations of the LuGre friction and Bouc-Wen models are presented in Table 8, where i is the input current, and f is the frequency. The subscript 'e' denotes parameters of the MRE component, while the subscript 'f' denotes those of the MRF component. The curve-fitted relations can portray the behavior of the model parameters at different loading conditions, which provide useful details during the system identification and control of semi-active devices, and ultimately, a generalized model of the H-MRE semi-active isolator can be developed.

6. Conclusion

In this study, a parametric model is proposed for the nonlinear and hysteretic behavior of a hybrid semi-active isolator that incorporates a hybrid MRE. The hybrid MRE is developed by encapsulating an MRF within the elastomer. Both conventional and hybrid MREs are fabricated and tested in experiments involving varying loading conditions of

excitation frequency and input current.

A single hysteresis model implementation for the hybrid MRE material would increase computational time and reduce prediction accuracy due to the significant number of parameters involved. Therefore, a parallel hysteresis model is used to improve the efficiency and accuracy of predicting the dynamic behavior of the hybrid MRE isolator. In the parameter identification process, a two-stage approach is employed. In the first stage, a single hysteresis model representing the C-MRE semi-active isolator is used. The models are simulated, and their responses are optimized to fit experimental data, resulting in optimized parameters for the MRE component in each of the three models. In the second stage, the MRF component parameters are identified using nine different Simulink models of the H-MRE semi-active isolator. Each of these models included two hysteretic components, which are combinations of Bouc-Wen, Modified-Dahl, or LuGre friction models. The parameters for the MRE hysteretic component are obtained from the first stage of the simulation. The models are then simulated, and the parameters for the MRF component are obtained by optimizing them to fit experimental data for the H-MRE semi-active isolator. This process identifies the best combination of the three proposed models.

The estimation results indicate that a combination of the LuGre friction model for MRE and Bouc-Wen for MRF is the most accurate in predicting the hysteretic response of the hybrid isolator. Furthermore, the study investigates the relationship between the selected model parameters and loading conditions to contribute to a field-dependent model by estimating the model response using experimental data with different excitation frequencies and input currents. Polynomial equations of the third order are used to describe these relationships, providing valuable insights for the system identification and control of hybrid semi-active isolators. The proposed model has the potential to be utilized in the design and control of smart base isolation systems with hybrid MREs, and future research can focus on exploring these possibilities.

Declaration of competing interest

The authors declare no conflict of interest.

Data availability

The authors do not have permission to share data.

Acknowledgement

References

Ali, A.M.H., et al., 2022. Effect of carbonyl iron particle types on the structure and performance of magnetorheological elastomers: a frequency and strain dependent study. Polym 14 (19), 4193, 2022, Vol. 14, *Page 4193*.

Ali, A., Salem, A.M.H., Muthalif, A.G.A., Bin Ramli, R., Julai, S., 2022. Development of a performance-enhanced hybrid magnetorheological elastomer-fluid for semi-active vibration isolation: static and dynamic experimental characterization. Mater 15 (9), 3238, 2022, Vol. 15, *Page 3238*.

Bastola, A.K., Hossain, M., 2020. A review on magneto-mechanical characterizations of magnetorheological elastomers. Compos. B Eng. 200, 108348.

Bastola, A.K., Paudel, M., Li, L., 2018. Development of hybrid magnetorheological elastomers by 3D printing. Polymer (Guildf). 149, 213–228. Aug.

Carlson, J.D., Jolly, M.R., 2000. MR fluid, foam and elastomer devices. Mechatronics 10 (4–5), 555–569. Jun.

Choi, H.J., Zhang, W.L., Kim, S., Seo, Y., 2014. Core-shell structured electro- and magneto-responsive materials: fabrication and characteristics. Vol. 7, Pages 7460-7471 Mater 7 (11), 7460–7471. Nov. 2014.

Dang, F., Enomoto, N., Hojo, J., Enpuku, K., 2010. Sonochemical coating of magnetite nanoparticles with silica. Ultrason. Sonochem. 17 (1), 193–199. Jan.

Díez, A.G., Tubio, C.R., Etxebarria, J.G., Lanceros-Mendez, S., 2021. Magnetorheological elastomer-based materials and devices: state of the art and future perspectives. Adv. Eng. Mater. 23 (6), 2100240. Jun.

Gao, P., Xiang, C., Liu, H., Walker, P., Zhang, N., 2019. Design of the frequency tuning scheme for a semi-active vibration absorber. Mech. Mach. Theor. 140, 641–653. Oct.

Hafeez, M.A., Usman, M., Umer, M.A., Hanif, A., 2020. Recent progress in isotropic magnetorheological elastomers and their properties: a review. Vol. 12 Polym 12 (12), 3023, p. 3023, Dec. 2020.

Jaafar, M.F., Mustapha, F., Mustapha, M., 2021. Review of current research progress related to magnetorheological elastomer material. J. Mater. Res. Technol. 15, 5010–5045, Nov.

Jang, D.I., Yun, G.E., Park, J.E., Kim, Y.K., 2018. Designing an attachable and power-efficient all-in-one module of a tunable vibration absorber based on magnetorheological elastomer. Smart Mater. Struct. 27 (8), 085009. Jul.

Jiménez, R., Álvarez-Icaza, L., 2005. LuGre friction model for a magnetorheological damper. Struct. Control Health Monit. 12 (1), 91–116. Jan.

Kang, S.S., Choi, K., Nam, J.-D., Choi, H.J., 2020. Magnetorheological elastomers: fabrication, characteristics, and applications, 2020, Vol. 13, Page 4597 Mater 13 (20), 4597. Oct.

Khurana, A., Kumar, D., Sharma, A.K., Joglekar, M.M., 2021. Nonlinear oscillations of particle-reinforced electro-magneto-viscoelastomer actuators. J. Appl. Mech. Trans. ASME 88 (12). Dec.

Khurana, A., Kumar, D., Sharma, A.K., Zurlo, G., Joglekar, M.M., 2022a. Taut domains in transversely isotropic electro-magneto-active thin membranes. Int. J. Non Lin. Mech. 147, 104228. Dec.

Khurana, A., Kumar, D., Sharma, A.K., Joglekar, M.M., 2022b. Static and dynamic instability modeling of electro-magneto-active polymers with various entanglements and crosslinks. Int. J. Non Lin. Mech. 139, 103865. Mar.

Koo, J.H., Dawson, A., Jung, H.J., 2012. "Characterization of actuation properties of magnetorheological elastomers with embedded hard magnetic particles:,". https://doi.org/10.1177/1045389X12439635 vol. 23, no. 9, pp. 1049–1054, Mar.

Li, Y., Li, J., 2019. Overview of the development of smart base isolation system featuring magnetorheological elastomer. Smart Struct. Syst. 24 (1), 37–52.

Li, Y., Li, J., Li, W., Du, H., 2014. A state-of-the-art review on magnetorheological elastomer devices. Smart Mater. Struct. 23 (12), 123001. Nov.

Muthalif, A.G.A., Razali, M.K.M., Nordin, N. H. Di, Hamid, S.B.A., 2021. Parametric estimation from empirical data using particle swarm optimization method for different magnetorheological damper models. IEEE Access 9, 72602–72613.

Qi, S., Guo, H., Fu, J., Xie, Y., Zhu, M., Yu, M., 2020. 3D printed shape-programmable magneto-active soft matter for biomimetic applications. Compos. Sci. Technol. 188, 107973. Mar.

Salem, A.M.H., Ali, A., Muthalif, A.G.A., Bin Ramli, R., Julai, S., 2021. Magnetorheological elastomer based flexible metamaterials coupler for broadband longitudinal vibration isolation: modeling and experimental verification. IEEE Access 9, 165451–165461.

Stepanov, G.V., Abramchuk, S.S., Grishin, D.A., Nikitin, L.V., Kramarenko, E.Y., Khokhlov, A.R., 2007. Effect of a homogeneous magnetic field on the viscoelastic behavior of magnetic elastomers. Polymer (Guildf). 48 (2), 488–495. Jan.

Sun, S.S., et al., 2014. The development of an adaptive tuned magnetorheological elastomer absorber working in squeeze mode. Smart Mater. Struct. 23 (7).

Ubaidillah, J. Sutrisno, Purwanto, A., Mazlan, S.A., 2015. no. 5. "Recent Progress on Magnetorheological Solids: Materials, Fabrication, Testing, and Applications," Advanced Engineering Materials, 17. Wiley-VCH Verlag, pp. 563–597, 01-May.

Yang, J., et al., 2013. Experimental study and modeling of a novel magnetorheological elastomer isolator. Smart Mater. Struct. 22 (11), 117001. Oct.

Yu, Y., Li, Y., Li, J., 2015. Parameter identification and sensitivity analysis of an improved LuGre friction model for magnetorheological elastomer base isolator. Meccanica 50 (11), 2691–2707. May.

Yu, Y., Li, Y., Li, J., Gu, X., 2016. A hysteresis model for dynamic behaviour of magnetorheological elastomer base isolator. Smart Mater. Struct. 25 (5), 055029. Apr.

Yu, Y., Li, J., Li, Y., Li, S., Li, H., Wang, W., 2019. Comparative investigation of phenomenological modeling for hysteresis responses of magnetorheological elastomer devices, 2019, Vol. 20, Page 3216 Int. J. Mol. Sci. 20 (13), 3216. Jun.

Zhou, Q., Nielsen, S.R.K., Qu, W.L., 2006. Semi-active control of three-dimensional vibrations of an inclined sag cable with magnetorheological dampers. J. Sound Vib. 296 (1–2), 1–22. Sep.

Carbonyl iron powder – made by its inventor! [Online]. Available: https://electronics-electric.basf.com/global/en/electronics/products/carbonyl_iron_powder.html. (Accessed 18 April 2023).

Elite Double 32 Fast - zhermack [Online]. Available: https://www.zhermack.com/en/product/elite-double-32-fast/. (Accessed 18 April 2023).